Nanoclusters of CaSe in calcium-doped Bi_2Se_3 grown by molecular-beam epitaxy

2016 Nanotechnology 27 085601

(http://iopscience.iop.org/0957-4484/27/8/085601)

IOP Publishing Nanotechnology
Nanotechnology 27 (2016) 085601 (6pp) doi:10.1088/0957-4484/27/8/085601

Nanoclusters of CaSe in calcium-doped Bi_2Se_3 grown by molecular-beam epitaxy

Panju Shang[1], Xin Guo[2], Bao Zhao[3], Xianqi Dai[3], Li Bin[2], Jinfeng Jia[4], Quan Li[1] and Maohai Xie[2]

[1] Department of Physics, The Chinese University of Hong Kong, Shatin, Hong Kong, People's Republic of China
[2] Department of Physics, The University of Hong Kong, Pokfulam Road, Hong Kong, People's Republic of China
[3] College of Physics and Electronic Engineering, Henan Normal University, Xinxiang, Henan 453007, China; and School of Physics and Electronic Engineering, Zhengzhou Normal University, Zhengzhou, Henan 450044, People's Republic of China
[4] Key Laboratory of Artificial Structures and Quantum Control (Ministry of Education); Collaborative Innovation Center of Advanced Microstructures, Department of Physics and Astronomy, Shanghai Jiaotong University, 800 Dongchuan Road, Shanghai 200240, People's Republic of China

E-mail: xqdai@henannu.edu.cn, liquan@phy.cuhk.edu.hk and mhxie@hku.hk

Received 8 October 2015, revised 17 December 2015
Accepted for publication 18 December 2015
Published 25 January 2016

Abstract

In calcium (Ca) doped Bi_2Se_3 films grown by molecular beam epitaxy, nanoclusters of CaSe are revealed by high-angle annular dark field imaging and energy dispersive x-ray spectroscopy analysis using a scanning transmission electron microscope. As the interface between the ordinary insulator CaSe and topological insulator, Bi_2Se_3, can host topological nontrivial interface state, this represents an interesting material system for further studies. We show by first principles total energy calculations that aggregation of Ca atoms in Bi_2Se_3 is driven by energy minimization and a preferential intercalation of Ca in the van der Waals gap between quintuple layers of Bi_2Se_3 induces reordering of atomic stacking and causes an increasing amount of stacking faults in film. The above findings also provide an explanation of less-than-expected electrical carrier (hole) concentrations in Ca-doped samples.

Keywords: topological insulator, nanoclusters, molecular-beam epitaxy, scanning transmission electron microscopy

(Some figures may appear in colour only in the online journal)

1. Introduction

Crystalline Bi_2Se_3 has been identified as one of the most promising three-dimensional (3D) topological insulators (TIs) and has received extensive research attention in recent years [1–17]. Its surface or interface with an ordinary insulator (OI) can host the nontrivial Dirac cone states with some interesting properties and future spintronic and quantum computing promises [2, 3, 18–22]. A bulk crystal of Bi_2Se_3 has a rhombohedral structure with the space group $R\bar{3}m$. Essentially, it is a layered compound composed of alternating stacks of Se and Bi atomic planes in the close-packed face-centered cubic stacking order. The unit cell of Bi_2Se_3 consists of, in the *c*-axis direction, three quintuple layers (QLs) of Se-Bi-Se-Bi-Se atomic planes stacked in the sequence of -[ABCAB]-[CABCA]-[BCABC]-, where […] donates one QL. Atoms within each QL are covalently bonded, whereas they interact via the weak van der Waals (vdW) forces between adjacent QLs.

Recently, great advances have been made in fabricating high-quality Bi_2Se_3 thin films by molecular-beam epitaxy (MBE) [4–10]. Properties of the TIs have been characterized extensively using thin film samples [2, 11–15]. One of the common features of the MBE-grown Bi_2Se_3 films is the unintentional *n*-type doping, presumably by some intrinsic defects such as Se-vacancies. Efforts have since been made to

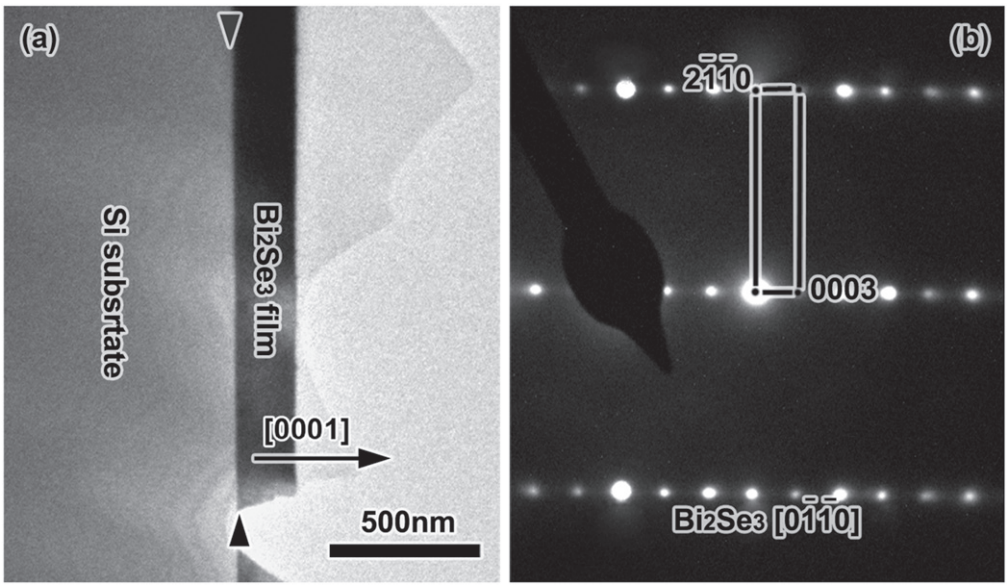

Figure 1. (a) Cross-sectional bright field TEM image and (b) selected area diffraction pattern of the Bi_2Se_3 thin film epitaxially grown on Si(111).

compensate electrons by introducing *p*-type dopants, such as Calcium (Ca), in order to tune the Fermi level and thereby to access the Dirac-cone states of the material. For example, *p*-type Bi_2Se_3 with hole concentrations of $\sim 10^{19}\,cm^{-3}$ have been reported by doping ~0.5% Ca in atomic concentrations [16, 17, 23]. However, a simple counting reveals that not all of the doped Ca atoms contribute to holes in Bi_2Se_3 and an appreciable amount must have remained electrically inactive with reasons uncounted so far.

Previous studies of the properties and physics of the TIs have focused primarily on surfaces (*i.e.*, their interfaces with vacuum). A notable exception is the recently reported Bi_2Se_3/In_2Se_3 superlattice sample, from which a 3D to two-dimensional (2D) crossover of quantum transport was revealed upon changing the constituent layer thickness [24]. An extension of the latter will be samples containing TI nanodots or clusters which may be achieved by embedding an OI in the matrix of a TI, or vice versa, for example. New effects and properties may be expected from such samples, and which may form an important and new front of TI research [25–27].

Here, in this study, we report an observation of nanoclusters of CaSe, an ordinary insulator [28], in the matrix of Bi_2Se_3 in Ca-doped Bi_2Se_3 film grown by MBE. By employing high resolution high-angle annular dark field (HAADF) imaging and energy dispersive x-ray spectroscopy (EDS) in a scanning transmission electron microscope (STEM) [29–31], we unveil Ca-enriched or aggregated regions in Bi_2Se_3:Ca, representing the secondary phase of cubic CaSe. First principles total energy calculations suggest preferential Ca intercalation in between the QL 'vdW gap', which then promotes substitution of the Bi atoms in the top Bi_2Se_3 QLs, leading to formation of CaSe clusters. Experiments further reveal that Ca intercalation induces a reordering of atomic stacking of Bi_2Se_3, and thus causes a higher concentration of stacking faults than undoped samples. This reordering is shown to lower the system energy by first principles calculations. The intercalated Ca atoms, and those in the CaSe clusters, do not contribute to holes and so these findings could explain the less-than-expected hole concentrations in Ca-doped samples.

2. Experimental details

Growth of Bi_2Se_3:Ca on Si(111) substrate was conducted in an Omicron MBE reactor using elemental Bi, Se and Ca sources in conventional Knudsen cells [5]. Nominally flat Si (111) was deoxidized at $\geqslant$1000 °C in vacuum for a clean (7 × 7) surface, after which a thin layer of InSe buffer was grown before depositing Bi_2Se_3 [31]. The growth temperature was 490 K and the film growth rate was 1 QL/min. The flux ratio between Se and Bi was 10 : 1 and that of Ca was ~0.7% of Bi. The high flux ratio between Se and Bi had been shown to lead to better quality epifilms of Bi_2Se_3, while that of Ca/Bi ~ 0.7% was chosen in order to be comparable with that of the literature and better chance to locate Ca atoms and precipitates by STEM studies [16, 17, 23]. The film thickness was ~200 nm and the hole concentration was $\sim 10^{19}\,cm^{-3}$ according to the Hall measurements.

High resolution STEM images were taken by the HAADF detector in a double corrected Titan microscope operated at 300 kV. The HAADF collection angle was 50–200 mrad. Cross-sectional TEM specimen was prepared by the standard method of mechanical thinning and Argon ion milling. Chemical mapping of the sample was done using the STEM energy dispersive x-ray (EDX) spectroscopy in a probe-corrected Tecnai microscope (operated at 200 kV) with the FEI super-X detector attached to the same microscope. The probe size was about 0.2 nm. The beam current was 0.3 nA.

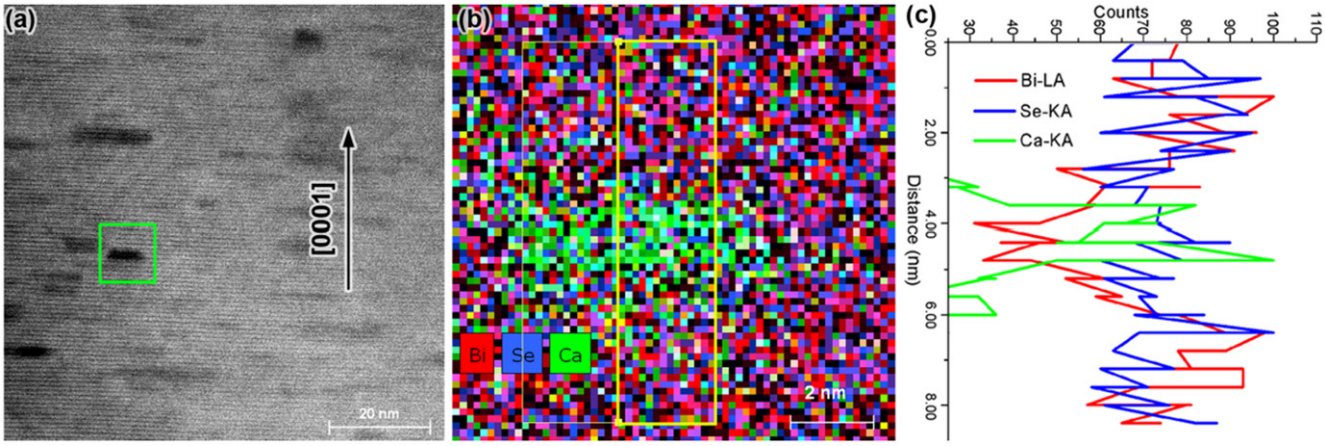

Figure 2. (a) Low magnification HAADF-STEM image taken along the [11$\bar{2}$0] Bi_2Se_3 zone axis showing the distinct light/dark contrast of Bi_2Se_3 thin film. (b) Overlapped elemental maps of Ca, Se, and Bi taken from the boxed region in (a). (c) The element profiles of the marked area in (b) showing the abundance of Bi, Se and Ca.

3. Results and discussions

We firstly established, by analysis of the selected area electron diffraction patterns (SAEDP), that epitaxial Bi_2Se_3 on Si (111) grows along the [0001] direction. Figure 1 shows a low magnification bright field (BF) TEM image and the corresponding SAEDP of the sample. The interface between Bi_2Se_3 and Si substrate is marked by the triangle arrows in figure 1(a). All diffraction spots in figure 1(b) can be indexed to the [0$\bar{1}\bar{1}$0] zone of Bi_2Se_3, signifying the single crystallinity of the film. After correcting the magnetic rotation angle between the BF image and the SAEDP, the growth direction of the epifilm is determined as along Bi_2Se_3 [0001].

HAADF-STEM images of the sample taken at low magnification (figure 2(a)) reveal regions of dark contrast in the Ca-doped Bi_2Se_3 film. As the contrast of HAADF-STEM image is roughly proportional to Z^n, where Z is the atomic number and n is a constant of 1.7–2 [29–31], the dark contrast regions in figure 2(a) indicate local enrichment of element(s) of lower atomic number than that of Bi and Se. We have examined the spatial distributions of the constituent elements, Bi, Se and Ca, in order to seek possible correlation between the chemical distribution and the contrast variation in the HADDF images. Figure 2(b) shows overlapping Bi, Se, and Ca chemical maps obtained by the STEM-EDX. It can be found that local enrichment of Ca in the chemical map matches well with the location of the dark contrast in the HAADF image, suggesting the correlation between the two. Based on the EDX results, one may plot the abundance profiles of the three elements (see figure 2(c) taken from the yellow-box region in figure 2(b)), which discloses another interesting feature: while Se concentration in the Ca-rich region is almost the same as that of the Ca-deficient region, Bi-deficiency coincides with the enrichment of Ca in locations having the dark contrast in the HAADF image. This implies that Ca takes the position of Bi in these regions and thus likely forms a second phase in the Bi_2Se_3 lattice. Figure 3 presents a high-resolution HAADF image close to a Ca-rich region. In this image, each bright dot represents the location of a Bi atom

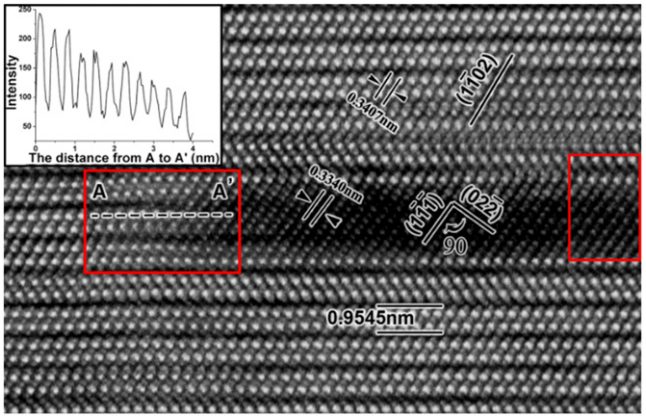

Figure 3. High resolution HAADF image showing the atomic structure of the dark region in figure 2(a). The inset presents the intensity profile along the AA′.

column while the slightly darker dot shows a Se column. As shown, away from the Ca-rich dark contrast region in the middle right, individual QLs of Bi_2Se_3 are clearly resolved and in each QL, three Se and two Bi atomic layers stack alternatingly in the ABCAB order. On the other hand, in the Ca-rich region, such repetitive QL structure has disappeared. The inter-plane spacing along two perpendicular dimensions are measured to be 0.33 nm and 0.22 nm, corresponding respectively to the (1$\bar{1}\bar{1}$) and (02$\bar{2}$) planes of cubic CaSe having the lattice parameter of $a = b = c = 0.592$ nm and $\alpha = \beta = \gamma = 90°$. Together with the chemical abundance of Ca (and deficiency of Bi), the switching from rhombohedral Bi_2Se_3 to cubic CaSe thus suggests that instead of the randomly distributed Ca atoms in Bi_2Se_3 acting as the dopant, many Ca atoms have aggregated and substituted Bi in that region, forming the cubic CaSe clusters in the host Bi_2Se_3 crystal. From the low magnification HAADF-STEM image of figure 2(a), we note that the CaSe clusters are quite abundant and statistical analysis of the CaSe cluster sizes in the STEM images provides an estimate of Ca concentration of $\leqslant$1%, which is not far from 0.7%. Ca in CaSe is not electrically

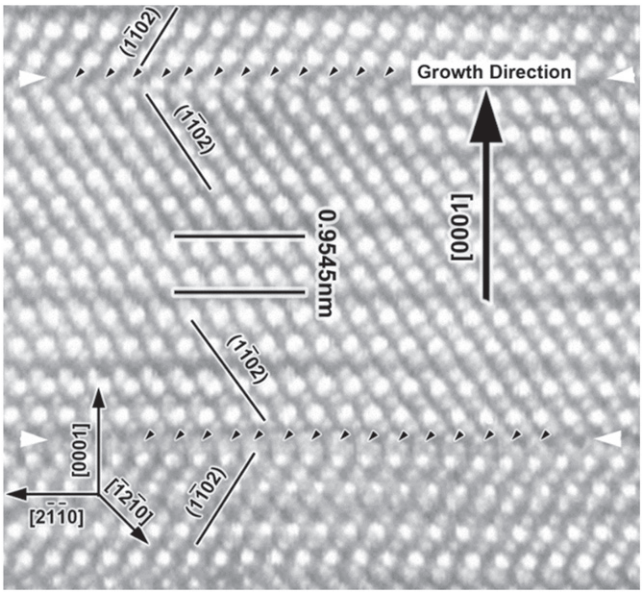

Figure 4. High resolution HAADF-STEM image taken along the $[11\bar{2}0]$ zone axis of Ca-doped Bi_2Se_3 thin film. Rows of small black arrows indicate intercalated Ca atoms, which induce the stacking order changes marked by the white arrows.

active and does not act as p-type dopant, so the above observation would explain the less-than-expected hole concentration in the Bi_2Se_3:Ca films. Interestingly, since crystalline CaSe is an ordinary insulator, nanoclusters of CaSe embedded in the matrix of Bi_2Se_3 generate internal TI/OI interfaces that will host nontrivial Dirac states, which invite future transport studies for new effects and physics.

From figure 3, we note that the insertion of CaSe clusters in the middle of the repetitive QL structure of Bi_2Se_3 has little effect on the growth pattern. Bi_2Se_3 grown above CaSe is seen to retain the same crystalline orientation as the rest of the Bi_2Se_3 lattice. A sharp boundary between Bi_2Se_3 and CaSe can be observed along the film growth direction. In contrast, the boundary between Bi_2Se_3 and CaSe perpendicular to the film surface is not that obvious. In regions marked by the red rectangles in figure 3, although the repetitive QL structure can be observed (suggesting the existence of the layered crystal structure of Bi_2Se_3), the intensity of Bi columns appears lower than those far away from the dark regions. The inset shown in the upper-left corner of the figure presents an intensity profile along AA′ as marked in the red rectangle box. The obvious intensity decay from A to A′ implies the evolution of partial replacement of Bi by Ca in the corresponding lattice sites. Crystallographic analysis of high resolution HAADF images reveals an apparent epitaxial relationship between the Bi_2Se_3 matrix and the CaSe precipitates, i.e., $[11\bar{2}0]_{Bi_2Se_3} \| [211]_{CaSe}$, and $[1\bar{1}02]_{Bi_2Se_3} \| [1\bar{1}\bar{1}]_{CaSe}$. The misfit of the interplanar spacing between $(1\bar{1}\bar{1})_{CaSe}$ and $(1\bar{1}02)_{Bi_2Se_3}$ planes is about ~2%, allowing incorporation of CaSe clusters without destroying the growth texture of Bi_2Se_3 along [0001].

Another feature observed by the TEM studies is the abundance of stacking faults in Bi_2Se_3:Ca films (notably higher in density than undoped samples). In the high-resolution HAADF-STEM image of figure 4, two stacking faults (marked by the white arrows) are easily recognized by the change of the stacking symmetry along the Bi_2Se_3 [0001] direction. It consists of a relative displacement along the $\langle 2\bar{1}\bar{1}0\rangle$ directions in the (0001) plane. Careful examinations of figure 4 at the stacking faults reveal layers of surplus atom precipitations (marked by the rows of small black arrows). Such layers of atoms can be associated with Ca atoms that precipitate in the vdW gap. It seems that Ca precipitation at the vdW interface will trigger the stacking-order change and thus results in stacking faults in the film.

In order to understand the above Ca-doping induced effects on epitaxial Bi_2Se_3, we performed the first principles total energy calculations using the Vienna *ab initio* simulation package (VASP) based on the density functional theory (DFT) [32, 33]. In the calculation, the electron-ionic core interaction were represented by the PAW potentials. The Perdew–Burke–Ernzerhof (PBE) formulation of the GGA was chosen to treat electron exchange and correlations. To simulate Bi_2Se_3 bulk environment, we constructed a slab consisting of 6 QLs using the experimental lattice constants of $a = 4.14$ Å and $c = 28.64$ Å and a vacuum region of 20 Å in the c-direction. The outermost 2 QLs on both sides of the slab are static, whereas the middle 2 QLs are free to relax. In all calculations, an energy cutoff of 340 eV is used for the plane-wave expansion of the wavefunctions. The reciprocal space is sampled with $9 \times 9 \times 1$ k-points grids, which are generated using the Monkhorst-Pack method.

We compared the formation energies between structures of one layer Ca atoms being inserted in the vdW gap (a and b in figure 5) and that of a layer of Ca substituting Bi(1) or Bi (2) or both of Bi_2Se_3 QL (figures 5(c)–(e)). We find that both configurations are possible from the formation energy point of view, but the former configuration, *i.e.*, Ca layer precipitated in the vdW gap, is favorable by over 2.2 eV in the Se-rich condition (which is the condition used in experiment) [34]. Therefore incorporation of Ca during MBE of Bi_2Se_3 is likely initiated by adsorption on the vdW surface and subsequently buried by the top-layer deposit. Interestingly, our calculations also show that upon inserting the Ca layer in the vdW gap, there is an energy gain of 79 meV when the Bi_2Se_3 lattice reverses its stacking order (*i.e.*, figure 5(b) versus figure 5(a)), which is in accordance with the experimental finding. Along with the Ca insertion layer in the vdW gap, substitutional doping of Ca at the Bi(1) and Bi(2) sites (see figures 5(c) and (d)) becomes more favorable, leading to an energy gain of 2.38 eV and 0.67 eV, respectively, over that when there is no Ca insertion-layer. This, firstly, suggests that there exists a tendency of Ca atoms to cluster by substituting the Bi atoms in Bi_2Se_3 directly above the Ca insertion layer. Secondly, the substitutional dopant preferably goes to the Bi(1) sites over the Bi(2) layer. Once the Bi(1) layer has been replaced by Ca atoms, further incorporation of Ca at the next Bi(2) layer results in an further energy reduction of 0.396 eV. In this way, Ca incorporation in Bi_2Se_3 appears 'catalytic', and proceeds by insertion initially at the vdW gap followed by substituting the Bi(1) and Bi(2) layers sequentially. This leads to

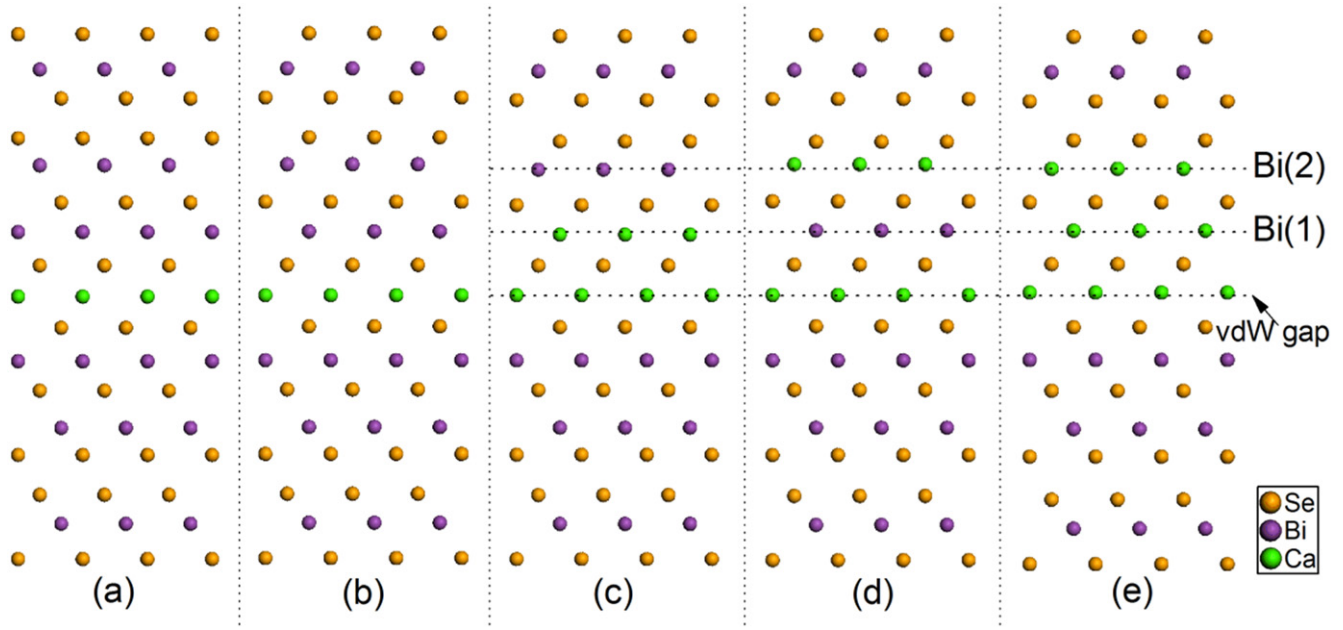

Figure 5. Schematic illustration of the structures of Ca-doped Bi_2Se_3. Intercalation of Ca into the vdW gap with the order of (**a**) –[ABCAB]-Ca-[CABCA]– and (**b**) –[ABCAB]-Ca-[CBACB]–. The substitution of Ca at the Bi(1) sites (**c**), Bi(2) sites (**d**) and simultaneously Bi(1) and Bi(2) sites (**e**) based on the structure in (b).

formation of a cubic phase CaSe in the matrix of Bi_2Se_3 as depicted in figure 5(e), consistent with the TEM observations.

4. Conclusion

By employing the HAADF-STEM, we identified distinctive morphological/structural features in Ca-doped Bi_2Se_3 films grown by MBE. Specifically, we observed nanoclusters of CaSe formed in the matrix of Bi_2Se_3. We also noted a stacking order change by Ca intercalation in the vdW gaps. From our total energy calculations, we suggest the possible mechanism responsible for the local segregation and clustering of CaSe. Ca atoms in CaSe clusters and intercalated in the vdW gaps do not contribute to holes, and this serves to explain the less-than-expected hole concentrations in Ca-doped Bi_2Se_3 films.

Acknowledgements

The authors are grateful to the technical assistance of Dr D Tang from FEI Co. MX and JJ acknowledge the support from a grant of the SRFDP and RGC ERG Joint Research Scheme of Hong Kong RGC and the Ministry of Education of China (No. M-HKU709/12).

References

[1] Zhang H, Liu C-X, Qi X-L, Dai X, Fang Z and Zhang S-C 2009 Topological insulators in Bi_2Se_3, Bi_2Te_3 and Sb_2Te_3 with a single Dirac cone on the surface *Nat. Phys.* **5** 438–42

[2] Hsieh D *et al* 2009 A tunable topological insulator in the spin helical Dirac transport regime *Nature* **460** 1101–5

[3] Xia Y *et al* 2009 Observation of a large-gap topological-insulator class with a single Dirac cone on the surface *Nat. Phys.* **5** 398–402

[4] Zhang G, Qin H, Teng J, Guo J, Guo Q, Dai X, Fang Z and Wu K 2009 Quintuple-layer epitaxy of thin films of topological insulator Bi_2Se_3 *Appl. Phys. Lett.* **95** 053114

[5] Li H D, Wang Z Y, Kan X, Guo X, He H T, Wang J N, Wong T L, Wang N and Xie M H 2010 The van der Waals epitaxy of Bi_2Se_3 on the vicinal Si(111) surface: an approach for preparing high-quality thin films of a topological insulator *New J. Phys.* **12** 103038

[6] He K *et al* 2010 Crossover of the three-dimensional topological insulator Bi_2Se_3 to the two-dimensional limit *Nat. Phys.* **6** 584–8

[7] Song C-L *et al* 2010 Topological insulator Bi_2Se_3 thin films grown on double-layer graphene by molecular beam epitaxy *Appl. Phys. Lett.* **97** 143118

[8] He L, Xiu F, Wang Y, Fedorov A V, Huang G, Kou X, Lang M, Beyermann W P, Zou J and Wang K L 2011 Epitaxial growth of Bi_2Se_3 topological insulator thin films on Si (111) *J. Appl. Phys.* **109** 103702

[9] Kou X F *et al* 2011 Epitaxial growth of high mobility Bi_2Se_3 thin films on CdS *Appl. Phys. Lett.* **98** 242102

[10] Bansal N *et al* 2011 Epitaxial growth of topological insulator Bi_2Se_3 film on Si(111) with atomically sharp interface *Thin Solid Films* **520** 224–9

[11] Pan Z-H, Vescovo E, Fedorov A V, Gardner D, Lee Y S, Chu S, Gu G D and Valla T 2011 Electronic structure of the topological insulator Bi_2Se_3 using angle-resolved photoemission spectroscopy: evidence for a nearly full surface spin polarization *Phys. Rev. Lett.* **106** 257004

[12] Cheng P *et al* 2010 Landau quantization of topological surface states in Bi_2Se_3 *Phys. Rev. Lett.* **105** 076801

[13] Hanaguri T, Igarashi K, Kawamura M, Takagi H and Sasagawa T 2010 Momentum-resolved Landau-level spectroscopy of Dirac surface state in Bi_2Se_3 *Phys. Rev.* B **82** 081305

[14] Analytis J G, Chu J-H, Chen Y, Corredor F, McDonald R D, Shen Z X and Fisher I R 2010 Bulk Fermi surface coexistence with Dirac surface state in Bi_2Se_3: a comparison of photoemission and Shubnikov–de Haas measurements *Phys. Rev.* B **81** 205407

[15] Chen J *et al* 2010 Gate-voltage control of chemical potential and weak antilocalization in Bi_2Se_3 *Phys. Rev. Lett.* **105** 176602

[16] Hor Y S, Richardella A, Roushan P, Xia Y, Checkelsky J G, Yazdani A, Hasan M Z, Ong N P and Cava R J 2009 p-type Bi_2Se_3 for topological insulator and low-temperature thermoelectric applications *Phys. Rev.* B **79** 195208

[17] Checkelsky J G, Hor Y S, Cava R J and Ong N P 2011 Bulk band gap and surface state conduction observed in voltage-tuned crystals of the topological insulator Bi_2Se_3 *Phys. Rev. Lett.* **106** 196801

[18] Nayak C, Stern A, Freedman M and Das Sarma S 2008 Non-Abelian anyons and topological quantum computation *Rev. Mod. Phys.* **80** 1083–159

[19] Akhmerov A R, Nilsson J and Beenakker C W J 2009 Electrically detected interferometry of majorana fermions in a topological insulator *Phys. Rev. Lett.* **102** 216404

[20] Moore J 2009 Topological insulators: the next generation *Nat. Phys.* **5** 378–80

[21] Qi X-L and Zhang S-C 2010 The quantum spin Hall effect and topological insulators *Phys. Today* **63** 33

[22] Moore J E 2010 The birth of topological insulators *Nature* **464** 194–8

[23] Checkelsky J G, Hor Y S, Liu M H, Qu D X, Cava R J and Ong N P 2009 Quantum interference in macroscopic crystals of nonmetallic Bi_2Se_3 *Phys. Rev. Lett.* **103** 246601

[24] Zhao Y *et al* 2014 Crossover from 3D to 2D quantum transport in Bi_2Se_3/In_2Se_3 superlattices *Nano Lett.* **14** 5244–9

[25] Linder J, Yokoyama T and Sudbø A 2009 Anomalous finite size effects on surface states in the topological insulator Bi_2Se_3 *Phys. Rev.* B **80** 205401

[26] Lu H-Z, Shan W-Y, Yao W, Niu Q and Shen S-Q 2010 Massive Dirac fermions and spin physics in an ultrathin film of topological insulator *Phys. Rev.* B **81** 115407

[27] Liu C-X, Zhang H, Yan B, Qi X-L, Frauenheim T, Dai X, Fang Z and Zhang S-C 2010 Oscillatory crossover from two-dimensional to three-dimensional topological insulators *Phys. Rev.* B **81** 041307

[28] Madelung O 2012 *Semiconductors: Data Handbook* (Berlin: Springer)

[29] Donnadieu P, Shao Y, De Geuser F, Botton G A, Lazar S, Cheynet M, de Boissieu M and Deschamps A 2011 Atomic structure of T1 precipitates in Al–Li–Cu alloys revisited with HAADF-STEM imaging and small-angle x-ray scattering *Acta Mater.* **59** 462–72

[30] Nellist P D and Pennycook S J 1999 Incoherent imaging using dynamically scattered coherent electrons *Ultramicroscopy* **78** 111–24

[31] Wang Z Y, Guo X, Li H D, Wong T L, Wang N and Xie M H 2011 Superlattices of Bi_2Se_3/In_2Se_3: growth characteristics and structural properties *Appl. Phys. Lett.* **99** 023112

[32] Kresse G 1996 Efficient iterative schemes for *ab initio* total-energy calculations using a plane-wave basis set *Phys. Rev.* B **54** 11169–86

[33] Kresse G and Hafner J 1993 *Ab initio* molecular dynamics for liquid metals *Phys. Rev.* B **47** 558–61

[34] Olin Å, Noläng B, Öhman L, Osadchii E and Rosén E 2005 Chemical thermodynamics of selenium *Chemical Thermodynamics* vol 7 (Amsterdam: Elsevier)